HUB-EP 97/96, KANAZAWA 97-23

to appear in PRD

Action and topological density carried by Abelian monopoles in finite temperature pure $SU(2)$ gauge theory: an analysis using RG smoothing *

E.–M. Ilgenfritz [1,2] †, H. Markum [3], M. Müller–Preussker [1], and S. Thurner [1,3]

[1] *Institut für Physik, Humboldt–Universität zu Berlin, Germany*

[2] *Institute for Theoretical Physics, University of Kanazawa, Japan*

[3] *Institut für Kernphysik, Technische Universität Wien, Austria*

We test a new parametrization of a suitably truncated classically perfect action for $SU(2)$ pure gauge theory with respect to self-consistency and locate the deconfinement transition on a $12^3 \times 4$ lattice. Using the technique of smoothing (blocking followed by inverse blocking) we demonstrate clustering of action and topological charge density. Concentrating on the Abelian monopoles found in smoothed configurations after Abelian projection from the maximally Abelian gauge, we present evidence for their role as carriers of non-Abelian action and topological charge.

PACS Numbers: 11.15.Ha, 12.38.Gc

---

*Supported by a Visitorship of S. T. to the Graduiertenkolleg 'Structure, Precision Tests and Extensions of the Standard Model of Elementary Particle Physics', GRK 271/1-96

†Supported by the Deutsche Forschungsgemeinschaft under grant Mu932/1-4

I. INTRODUCTION

Already for more than two decades the vacuum state as well as the finite-temperature structure of QCD have been viewed in terms of different kinds of topological excitations, instantons and Abelian monopoles. On one hand, instantons explain chiral symmetry breaking, play an important role within the axial anomaly and more generally, they provide a successful model for a wide range of applications in non-perturbative QCD phenomenology (for references see [1–4]). However, as long as (anti-) instantons are considered to form a dilute medium, they are hardly explaining the confinement of quarks. On the other hand, confinement can be reasonably based on a dual superconductor scenario invented by 't Hooft and Mandelstam [5,6]. Similarly as Cooper pairs form a condensate in a real superconductor, Abelian (anti-) monopoles occurring in pure Yang-Mills theories as singularities of an appropriate gauge condition are thought to condense and to lead to confinement through a color-electric dual Meissner effect. Lattice computations carried out by different groups [7–9] provided increasing evidence that, at least in the maximally Abelian gauge, the projected $U(1)$ degrees of freedom are the carriers of the long-range physics and that monopoles really seem to condense [10,11].

For a long time, these pictures of the QCD vacuum were not linked to each other. Only very recently it became more and more clear, that instantons, monopoles and dyons, respectively, are closely related [12–14]. The correlation becomes especially clear, when - after minimizing the classical action of previously Monte Carlo generated quantum gauge fields - (approximate) classical field configurations are approached.

In this paper we are going to investigate this interrelation in more detail within pure $SU(2)$ lattice gauge theory at finite temperature. We will apply a lattice formulation with fixed-point action which was invented in order to keep the lattice theory as close as possible to continuum physics. One virtue of the fixed-point action approach is that it has made it possible to treat topological excitations like instantons in a proper way [15–17]. Moreover, such formulations are based on renormalization group blocking and inverse blocking trans-

formations. This allows to give a precise definition of the scale of ultraviolet fluctuations which are integrated out from the gauge fields and how to change this scale [17,18]. For inverse blocking this statement holds as long as only one inverse blocking step is performed.

In a recent paper the present authors, together with M. Feurstein [19], proposed to use the inverse blocking method as a general tool suppressing ultraviolet fluctuations, in particular in order to expose the medium- and long-range physics in generic non-Abelian lattice gauge field configurations.

The concept of inverse blocking originally arose within the context of a classically perfect lattice action and has been essential for the construction of the perfect action or suitably truncated actions of less complexity [18]. The concept was then used to handle the otherwise difficult problem of defining *the* topological charge of a given lattice configuration [17]. The actual measurement of topological charge was based on a geometric method.

In the meantime, the method has been refined by repeating several steps of subsequent blocking (superimposing each time different coarse lattices) and inverse blocking ('smoothing cycles') [20] with the aim to resolve the instanton structure of individual lattice configurations. Doing that, strictly speaking, these authors gave up the original idea of inverse blocking, which was to preserve the structure of a given lattice configuration at any scale above the upper blocking level. Applying smoothing cycles - in a way very similar to the standard minimization of the gauge field action ('cooling') - does not only wipe out short-range fluctuations of perturbative origin but destroys also small-size non-perturbative structures (e.g. small instantons and distorted instantons in the real vacuum) that one might want to study. Not unexpectedly, the gauge fields are driven into configurations which exhibit well-separated lumps of action and topology. Near to their centers, these lumps can be well interpreted as single instantons frozen out of the lattice configurations. But there remained a puzzle [20]. Similar to moderate cooling, sufficiently large Wilson loops evaluated on the smoothed lattice gauge field configurations were still showing an area law with non-vanishing string tension. However, if one mocks up the gauge fields as dilute instanton gas configurations, taking the positions and sizes from the frozen out instantons, one fails to produce

confinement. Something seems to be lost.

The original Refs. [17] have been our starting point to look into more details of the description of lattice topology going beyond the measurement of the total topological charge. As in Ref. [19], we prefer in our present work the original point of view that one should preserve the structure of the gauge fields - as it is given in the quantized vacuum above the blocked level - by doing just *one* smoothing step.

From the very beginning, instead of studying the distribution of topological charge alone, we have been also interested in the monopole degrees of freedom and their interrelation with the topological density [19]. In that paper we have found that by the minimal smoothing procedure the noise of the topological density as well as the number of Abelian monopole currents become considerably reduced while the string tension changes only insignificantly.

This is challenging since it seems to indicate that the bulk of the monopole activity is *not* related to the property of confinement. For instance, in the result of smoothing (after removal of most of the abundant monopoles) the finite temperature anisotropy of the remaining monopole currents becomes enhanced and behaves qualitatively like an order parameter of the confinement/deconfinement transition. In the deconfined phase, only very few space-like monopole currents remain on the smoothed lattice configurations.

In Sections II and III of the present work we prove the stability of a new parametrization of the fixed-point gauge action and determine the coupling β_{crit} where the deconfinement transition occurs for our $N_\tau = 4$ lattice. In the following Sections IV and V we provide additional evidence that a gauge invariant characterization of the Abelian monopole degrees of freedom is possible. We point out local correlations between the monopole currents of the maximally Abelian gauge and the local action and the local topological density. These signals are enhanced for smoothed configurations. Finally, we conclude and propose directions for further investigations in Section VI.

II. TESTS FOR OPTIMIZING THE ACTION

The simplified fixed-point action [17] has been improved recently, and a suitably truncated version [21] has been obtained. Again, it is parametrized in terms of only two types of Wilson loops, plaquettes $U_{C_1} = U_{x,\mu,\nu}$ (type C_1) and tilted 3-dimensional 6-link loops (type C_2) of the form

$$U_{C_2} = U_{x,\mu,\nu,\lambda} = U_{x,\mu} U_{x+\hat{\mu},\nu} U_{x+\hat{\mu}+\hat{\nu},\lambda} U^+_{x+\hat{\nu}+\hat{\lambda},\mu} U^+_{x+\hat{\lambda},\nu} U^+_{x,\lambda} \ , \tag{1}$$

and contains several powers of the linear action terms corresponding to each loop of both types that can be drawn on the lattice

$$S_{FP}(U) = \sum_{type} \sum_i \sum_{C_i} \sum_{j=1}^{4} w(i,j) (1 - \frac{1}{2} \ \mathrm{Tr} \ U_{C_i})^j \ . \tag{2}$$

The parameters of this action have changed [21] compared to [17] and are reproduced in Table I.

Suppose we have a fine lattice of links U and a coarse lattice of links V covering the same physical volume. Being a classically perfect action, S_{FP} can be evaluated on both lattices and must satisfy the following condition

$$\mathrm{Min}_U \left(S_{FP}(U) + \kappa \ T(U,V) \right) = S_{FP}(V) \ , \tag{3}$$

configuration by configuration over a representative ensemble of equilibrium gauge field configurations V, near to the continuum limit. In other words, the minimum of the expression in brackets on the left hand side must saturate the lower bound provided by the right hand side. $T(U,V)$ is a certain non-negative functional related to the blockspin transformation (see [17,19]). Blocking means a mapping from the link fields U given on the fine lattice on link variables V which ought describe the same configuration on the next coarser lattice. This mapping is realized by the following construction:

$$\begin{aligned} \tilde{V}_{x,\mu} = & \ c_1^{block} \ U_{x,\mu} U_{x+\hat{\mu},\mu} \\ & + \sum_{\nu \neq \mu} c_2^{block} \Big(U_{x,\nu} U_{x+\hat{\nu},\mu} U_{x+\hat{\nu}+\hat{\mu},\mu} U^+_{x+2\hat{\mu},\nu} \\ & \qquad + \ U^+_{x-\hat{\nu},\nu} U_{x-\hat{\nu},\mu} U_{x-\hat{\nu}+\hat{\mu},\mu} U_{x-\hat{\nu}+2\hat{\mu},\nu} \Big) \ . \end{aligned} \tag{4}$$

The coarse link variable $V_{x,\mu}$ has to be an $SU(2)$ group element which requires normalization

$$V_{x,\mu} = \frac{\tilde{V}_{x,\mu}}{\sqrt{\det\left(\tilde{V}_{x,\mu}\right)}} \ . \tag{5}$$

The blocking parameters

$$\begin{aligned} c_2^{block} &= 0.12 \\ c_1^{block} &= 1 - 6\ c_2^{block} \end{aligned} \tag{6}$$

have been optimized earlier in Ref. [15] under very general conditions.

Inverse blocking is a mapping $V \to U^{SM}$ where the new link variables $U = U^{SM}$ are implicitly defined as the set of links providing, for the configuration encoded as V, the 'smoothest interpolation' on the next finer grained lattice. Practically, the link field U^{SM} must be found by minimizing the extended action in the bracket on the left hand side of Eq. (3). It is smoother than all possible *quantum* fields U from which the coarse level field V might have been obtained by blocking. From the point of view of minimization, κ plays the role of a Lagrange multiplier defining the strength of the constraint provided by the coarse grained configuration. The relation (3) expresses the equality of the fine and coarse grained partition functions within the saddle point approximation neglecting one-loop corrections (which holds in the classical limit for $\beta \to \infty$).

In our last paper [19] we encountered a problem that we could not resolve and which has caused some discussion. On one hand we used the action proposed in Ref. [17]. With this action we have generated our Monte Carlo configurations on the *fine lattice*. These have been blocked in order to get the ensemble of coarse configurations V. Then we did the minimization to yield the respective smoothed copies U^{SM} corresponding to each Monte Carlo configuration U^{MC}, again on the fine lattice. On the other hand, however, in order to match the condition of saturation (3) between the blocked and smoothed configurations on average in our Monte Carlo ensemble, we were forced to empirically tune κ to another (smaller) effective value. Thus, we were effectively working with a weaker constraint. Although we could make a number of valuable physical observations, this was not satisfactory,

because all parameters of the extended action are strongly related to each other by the very construction of this action.

Therefore, it was of primary importance for us to make an independent check of the new parametrization of the perfect action using our best minimization procedure. Before presenting the results of this test and the comparison with the old parametrization, some details on our minimization routine used to accomplish the inverse blocking are due at this place. There are two modes of relaxation which differ in the way how a tentative update of the whole lattice is proposed. They are tried one after another. The first mode consists in determining the direction of search for each link using the derivative with respect to U of the *linear part* of the extended action $S_{FP}(U) + \kappa T(U, V)$ occurring on the left hand side of Eq. (3). Then we try a quadratic interpolation of the extended action (now including the *non-linear terms in* S_{FP}) as function of the given link along the corresponding geodesics in $SU(2)$. This interpolation is based on action measurements for two step sizes (rotation angles) and is used to estimate an optimal angular step. This rotation is then applied to the link U as a tentative update. After all links are updated sequentially in this way, a global check is made whether the *full extended action* (including now the full blocking kernel $T(U, V)$) would really decrease. If this is the case, the tentative global update is accepted. If not, the second relaxation mode is chosen. Now the direction of search is chosen randomly in order to explore the neighborhood of the given link U in the gauge group. With respect to these directions a quadratic interpolation in the step size is constructed, too, in order to get an optimal rotation angle. If this global step leads to a smaller value of the full extended action, the proposed update is accepted. If not, the random search mode is repeated up to 5 times. In the test runs, we made up to 15 attempts in this mode. In most cases the first relaxation mode immediately leads to a successful update.

The test of the two actions has been done for 100 Monte Carlo configurations on a 12^4 lattice at $\beta = 2.5$. The two samples that we have to compare with respect to Eq. (3) were obtained with the standard Metropolis algorithm after 1000 thermalization steps, the configurations measured were separated by 100 sweeps. The first one is obtained from the

original Monte Carlo ensemble (created as U^{MC}) by blocking to $V(U^{MC})$. The second sample is obtained from the first by relaxation (with $\kappa = 12$) towards the smoothed $U^{SM}(U^{MC})$ fields. We show in Fig. 1, for the new parametrization given in Table I, the Monte Carlo history of the blocked action $S_{FP}(V)$ together with the respective minimum of the extended action $S_{FP}(U^{SM}) + \kappa T(U^{SM}, V)$. Average and standard deviation of the blocked action $S_{FP}(V)$ are 1988 ± 25 and for the minimum of the extended action $S_{FP}(U^{SM}) + \kappa T(U^{SM}, V)$ average and standard deviation are 2024 ± 30. For the difference $S_{FP}(U^{SM}) + \kappa T(U^{SM}, V) - S_{FP}(V)$, evaluated for respective blocked and smoothed configurations, we find 36 ± 6. These numbers give an impression how well the smoothed configurations represent the blocked ones. The old parametrization of the action has, for comparison at the same $\beta = 2.5$, average and standard deviation 1509 ± 25 for $S_{FP}(V)$, 1869 ± 28 for the minimal extended action $S_{FP}(U^{SM}) + \kappa T(U^{SM}, V)$ and 360 ± 5 for the difference. These results show to what extent the new action is better. It is not completely perfect, however, as it cannot be so at any finite β.

To get a feeling how sensitive the coefficients of the action are with respect to an attempted further improvement we considered the following. The left hand side of (3) depends on the parameters of the action not only explicitly, but also through the selection of Monte Carlo configurations U^{MC} and through the result of relaxation, U^{SM}. The dependence on the action coefficients is explicit only in $S_{FP}(V)$. Measuring the different contributions to the fixed-point action S_{FP} for the configurations U^{SM} and V one can now try to optimize the - deliberately free - parameters $\tilde{w}(i,j)$ in some modified action $\tilde{S}_{FP}(V)$ by minimizing the following error functional

$$\sum_{U^{MC}} \left\{ \tilde{S}_{FP}\left(V(U^{MC})\right) - S_{FP}\left(U^{SM}(U^{MC})\right) - \kappa\, T\left(U^{SM}(U^{MC}), V(U^{MC})\right) \right\}^2 / \sum_{U^{MC}} 1 \ . \quad (7)$$

The average is over our test sample of configurations. The $\tilde{w}(i,j)$ are chosen initially at random near to $w(i,j)$ and then they are let to evolve to minimize the error functional (7). This minimum turns out to be $\Delta S_{FP} = 4.98$ in the case of the new parametrization (applied to the fine lattice) and $\Delta S_{FP} = 6.21$ for the old one. More importantly, this requires small

relative changes of the parameters $\tilde{w}(i,j)$ in the case of the new action, typically $\simeq 1$ percent, 6 percent for the worst critical coupling $w(2,1)$. For the old parametrization the relative changes vary from $O(10)$ percent up to $O(100)$ percent for the most critical $w(2,1)$ and $w(2,4)$. In this sense, the new parametrization can be considered as much more stable.

In contrast to [19], the theoretically favored value of $\kappa = 12$ has been used in these tests and throughout the further investigations reported in this paper. We emphasize again the improvement achieved with the new parametrization [21] compared to the old one [17]. In the present work the new parametrization of the fixed-point action has been systematically tested and, to our knowledge for the first time, practically used for the topological analysis of equilibrium lattice configurations.

III. SEARCH FOR THE DECONFINEMENT TRANSITION

We have simulated thermal configurations with the new parametrization of the simplified fixed-point action at six β values in the interval $[1.52, 1.56]$ on lattice sizes $L^3 \times 4$ with $L = 8, 10$ and 12. The statistics covered 1000 configurations for the β values at the ends of the interval and 5000 for the four interior β values. The measurements were always separated by 20 Monte Carlo sweeps using the Metropolis algorithm. We have checked that the autocorrelations for the observables considered in the following were sufficiently suppressed. We examined the intersection of the Binder cumulants of the volume–averaged Polyakov loop P

$$B_4(L) = \frac{\langle P^4 \rangle}{\langle P^2 \rangle^2} - 3 \tag{8}$$

measured on the three lattices, respectively. For simplicity the result is shown only for $L = 8, 12$ in Fig. 2, in the upper part for the cumulant $B_4^U(L)$ expressed in terms of the Polyakov loop calculated from the U^{MC} (*not* from the smoothed configuration) on the fine lattice *and* in the lower part the cumulant $B_4^V(L)$ in terms of the Polyakov loop calculated from the blocked links V. These (unblocked and blocked) cumulants behave very similar which

gives independent support for the block spin transformation used. We find the crossings of the Binder cumulants for the three L values with each other to occur within the same interval $\beta_{crit} \in [1.535, 1.550]$, both for the unblocked $B_4^U(L)$ and the blocked $B_4^V(L)$. The corresponding values of the Binder cumulants have been seen to vary roughly in between -1.3 and -1.6 . There is an approximate agreement of $B_4^U(L)$ and $B_4^V(L)$ at β_{crit} with the value of $B_4(L)$ expected from the $3d$ Ising model (see [22]). This gives an indication that the finite temperature pure $SU(2)$ theory with the perfect action could also belong to the usual three-dimensional $Z(2)$ spin model universality class.

In other words, the ensemble of blocked configurations analyzed by means of the cumulant crossing criterion for the thermal phase transition points to the same value of β_{crit} as on the fine lattice where the actual simulations have been carried out. Notice that the coarse lattice has only $N_\tau = 2$ temporal lattice steps. We expect that the finite temperature results of a simulation on such a coarse lattice would suffer from bigger discretization errors. In any case, sizes of the fine lattice similar to that used in this study are certainly too small to draw any conclusions with respect to the finite size scaling behaviour of the model.

Before entering a thorough study over a broad range of temperatures including the immediate neighborhood of the deconfinement temperature, we will content ourselves in the present work with explorations at two temperatures, one in the confinement region corresponding to $\beta = 1.4$ and one deeply in the deconfinement phase at $\beta = 1.8$. We are aware that these cases are relatively far from the actual transition temperature. The linear extension of the lattice at $\beta = 1.8$ changes roughly by a factor one half compared with the lower β value.

IV. CLUSTERING OF ACTION AND TOPOLOGICAL CHARGE IN SMOOTHED CONFIGURATIONS

In this Section we will show that already the procedure of minimal smoothing (one blocking followed by one inverse blocking step) exhibits the clustering of topological charge

and action. On the $12^3 \times 4$ lattice used for our finite temperature investigation, at lower β values compared to the tests of the action, the inverse blocking does not reach that degree of saturation of Eq. (3) as decribed above. In comparison with Fig. 1 the two histories are somewhat more displaced from each other, and the remaining difference amounts to a few percent of $S_{FP}(V)$ depending on β.

The full topological analysis was done for only 50 configurations at both temperatures. We define the action density $s_{site}(x)$ per lattice point (also called 'local action') as follows

$$s_{site}(x) = \sum_{j=1}^{4} \left(\sum_{C_1(x)} \frac{w(1,j)}{4} (1 - \frac{1}{2} \text{ Tr } U_{C_1(x)})^j + \sum_{C_2(x)} \frac{w(2,j)}{6} (1 - \frac{1}{2} \text{ Tr } U_{C_2(x)})^j \right) . \qquad (9)$$

Here, according to the notation in Section II, $C_j(x)$ (with $j = 1, 2$) means loops of type j running through the lattice site x. Summing up $s_{site}(x)$ with respect to x yields the total action. The topological charge density definitions we are using are the naive one constructed out of plaquettes around a site x

$$q(x) = -\frac{1}{2^9 \pi^2} \sum_{\mu,\nu,\sigma,\rho=-4}^{+4} \epsilon_{\mu\nu\sigma\rho} \text{tr} \left(U_{x,\mu,\nu} U_{x,\sigma,\rho} \right) \qquad (10)$$

or the contribution from a given hypercube according to Lüscher's definition of charge [23]. We did not attempt to improve the field theoretic definition. Both topological densities used are known to behave regularly for smooth configurations [19].

The sequence of both (smoothed) charges is shown for $\beta = 1.4$ as an example for the confinement phase in Fig. 3 and subsequent configurations seem to be reasonably decorrelated. The ensemble has a dispersion of topological charges $\langle Q^2 \rangle = 9.04$ in case of the integer valued Lüscher charge and $\langle Q^2 \rangle = 7.14$ for the naive topological charge.

Figs. 4 show, in a 12×4 array of sub-pictures, each depicting 12×12 lattice points forming an xy plane, the clustering of the topological charge after smoothing. Figs. 4a, b correspond to a $Q = 0$ configuration obtained in the confinement phase. The majority of configurations has total charge $Q \neq 0$ but does not look qualitatively different from the shown example. The pattern of topological clusters is very rich. It is shown here together with the few monopole world lines remaining after smoothing. (Anti-) monopoles running

in one of the xy planes are shown by vertical and horizontal arrows. Time-like (anti-) monopoles are symbolized by arrows to (from) the upper right, space-like (anti-) monopoles with world lines in the z direction by arrows to (from) the upper left.

Figs. 4c, d show in the same way a smoothed configuration with total charge $Q = 0$ obtained at $\beta = 1.8$ in the deconfinement phase. It illustrates that the still existing, diluted topological charge is clustered in more perfect instanton-like shape and how the monopole world lines are correlated with these clusters.

It is visible that our minimal smoothing method gives clear evidence for clustering of the topological density at a scale of several lattice spacings in any possible section of the lattice in both phases. The topological density appears as a sufficiently smooth function in all Euclidean coordinates. However, a clear interpretation or parametrization in the form of instantons seems hardly possible in the confinement phase. Taking the action instead of the topological density, a similar behavior is observed.

This means that our minimal variant of smoothing is not biased in favor of nearly classical solutions of instanton shape. Nevertheless, as Fig. 5 shows, strong fields are preferably selfdual or antiselfdual. Physically, this indicates that the (anti-) instantons entering the dense fluid become strongly deformed under the influence of quantum fluctuations. A local analysis reveals that nearly selfdual or antiselfdual domains are clearly preferred in both phases as far as the local action exceeds a threshold value of $s_{site}(x) \approx 0.3$. This is documented by the ridges in the probability distribution of the local topological charge at given local action density which is shown in Fig. 5. It is not surprising that - at all β values in a manner similar to the continuum - the topological density is locally bounded by the action density

$$\frac{8\pi^2}{g^2} \, |q(x)| \leq \beta \cdot s_{site}(x) \, . \tag{11}$$

More than that, we find an enhanced probability to find a topological density near to saturation. This means that after smoothing strong enough color-electric and -magnetic fields show up mutually aligned to a high degree.

V. GAUGE INVARIANT PROPERTIES OF ABELIAN MONOPOLES

In our previous paper [19] we have performed the transformation to the maximal Abelian gauge of smoothed configurations U^{SM} and, for comparison, of the Monte Carlo configurations U^{MC} they originated from. After the projection to the Abelian gauge field (neglecting the charged vector matter fields in the non-diagonal components of the links) [7], the Abelian monopole content of the original Monte Carlo ensemble and of the ensemble of smoothed copies thereof has been determined by the DeGrand–Toussaint construction [24] as usual.

Our most astonishing result was that the monopole activity was reduced by more than an order of magnitude, roughly proportional to the reduction of the topological activity. The latter has been defined in Ref. [19] as $A_t = \sum_x |q(x)|$ in terms of the local topological density. Although the correlation function of monopole currents and topological density (given as a function of distance) was measurable also without smoothing, it was not different in shape (different in normalization, of course) for Monte Carlo and smoothed configurations.

We give now more detailed evidence for the local correlation of gauge invariant quantities (topological charge density and action density) with the presence of monopole currents. We have already illustrated the occurrence of (anti-) monopoles among the clusters of topological charge by plotting their world lines on the dual lattice in Figs. 4a, b in the confinement phase and in Figs. 4c, d in the deconfinement phase. Now we want to make these observations more quantitative. We did not consider here in detail the problem of non-uniqueness when fixing the maximal Abelian gauge (cf. [9]).[1] Instead, we have driven the corresponding gauge functional into a local extremum in the standard way. Our convergence criterium was chosen in such a way that we stopped the gauge fixing when the local relative changes of the gauge fixing functional become globally less than $O(10^{-8})$. In the average for smoothed configurations, this has required 620 (690) $\pm$ 250 gauge cooling iterations for $\beta = 1.4$ (1.8).

[1] Circumstancial evidence shows that the monopole currents can be displaced by one lattice spacing from one gauge copy to the other.

The number of gauge cooling iterations necessary for original Monte Carlo configurations to reach the same accuracy was only slightly bigger.

Fig. 6 shows in its upper part how, in smoothed configurations, the average occupation number of magnetic monopoles $\langle m(x)\rangle = \langle \sum_{dual\ links\ l\ next\ to\ x} |m_l| \rangle$ on nearest dual links depends on the local action available. There are 32 dual links nearest to a given lattice point. Here, the lattice points of all 50 configurations obtained at $\beta = 1.4$ have been classified according to their local action. For each bin the average number of monopole currents per lattice point has been calculated. The lower part of Fig. 6 shows the dependence of the average number of monopole currents on the local topological charge density for $\beta = 1.4$.

Apart from obvious changes in the scale of the action density, generically the same dependence occurs for $\beta = 1.8$ in the deconfinement phase. For instance, the range of the distribution of the local action values varies with β. In contrast to this, there are practically no lattice points with topological density $|q(x)| > 0.05$, irrespective of β. A physically relevant feature in Fig. 6 is the increase of the average local density of monopole currents $\langle m(x)\rangle$ at small action density $s_{site}(x)$ or topological density $|q(x)|$. For somewhat larger values of $s_{site}(x)$ and $|q(x)|$, respectively, the mean local monopole density seems to reach a plateau of one monopole current on the average. The increase of the error bars with s_{site} or $|q|$ reflects the insufficient statistics of lattice points with larger action or topological density.

Turning our point of view, we will now give a characterization of Abelian monopole currents in terms of locally defined *gauge independent* observables. We consider the 3-cubes of the original lattice dual to an elementary piece of monopole world line (a link of the dual lattice). This leads us to a natural definition of a local action on the monopole world line, $s_{3-cube}(c)$ instead of $s_{site}(x)$. We include into $s_{3-cube}(c)$ the contribution of all plaquettes forming the 6 faces of the 3-cube c plus the contribution of all 6-link loops which wind around its surface. In short, it is exactly the part of the total action which lives on that cube. Histograms of this local cube–oriented action $s_{3-cube}(c)$ after smoothing are shown in Fig. 7, separately for time-like and space-like dual links depending whether they are occupied by monopole currents or not. Of course, the range of values of $s_{3-cube}(c)$ spanned

by these distributions depends on β. All distributions are normalized to one, such that the different numbers of cubes entering each histogram are not directly visible. In the confinement phase, the direction (time-like or space-like) of the dual link obviously does not matter. The average of the local action and the square root of its variance $\langle \Delta s_{3-cube}(c)^2 \rangle$ are clearly bigger if the link carries a monopole current. This is qualitatively different in the deconfinement phase. The rare space-like monopole currents are always associated with a low local action while the time-like monopole currents have twice as large average action and bigger variance.

Fig. 8 analogously shows the histograms of a locally summed topological charge, separately for time-like and space-like dual links, occupied by a monopole current or not. The sum over $q(x)$ includes here the 8 corners of the 3-cube and should capture a total charge inside of some domain around the cube (centered in a hyperplane orthogonal to the direction of the dual link). The variance of the distribution is bigger for monopole cubes than for empty cubes, and is independent of the direction of the monopole current in the confinement phase. In the deconfinement phase, the variance of the local topological charge is also bigger around cubes with monopoles. Remember that the histograms shown here are all normalized to one independent of the fact that there are only very few space-like monopoles (see below).

Smoothing is important to exhibit more clearly the action and topological charge carried by the Abelian monopoles. In order to demonstrate this by comparison, we present data for unsmoothed configurations in Fig. 9, only for one coupling at $\beta = 1.4$. Notice the order of magnitude change in the scale of the local action $s_{3-cube}(c)$ compared to the plots for smoothed configurations (Fig. 7). Even without smoothing, there is a small but clear distinction in the distribution of the cube–oriented local action between monopole cubes and cubes without monopoles. In the topological density histograms, however, one cannot see any difference between the presence and absence of a monopole current as long as no smoothing has been performed. This does not mean the absence of correlations between monopoles and topologically charged objects, it only reflects that the topological density is

hidden by quantum fluctuations.

It seems to be natural to define an excess of action or topological charge per monopole world line length. This should be possible (independent of the configuration) if monopoles were semi-classical objects. We define this as the mean of the local action s_{3-cube} over all cubes which are dual to a monopole–occupied dual link in a given configuration. In the case of the topological charge we use the mean of the geometric topological charge over all $4d$ hypercubes from which a monopole current emanates. Again, we study this separately for space-like and time-like monopole currents.

In Figs. 10 and 11 we compare the mean action and topological charge per monopole world line length defined for the 50 individual configurations in the samples of lattice configurations generated at $\beta = 1.4$ and $\beta = 1.8$, respectively. The abscissa numbers the subsequent (smoothed) configurations. The ordinate of the symbols represents the mean local action or mean local topological charge per length of monopole world line in the configuration. Circles refer to space-like and crosses to time-like pieces of monopole world lines (monopole currents).

Let us first look at the case of confinement (Fig. 10). There is again no statistically significant difference between time-like and space-like monopole currents. The mean local action and the mean local topological charge per length fluctuate strongly from configuration to configuration. This means that under the given circumstances there is no sharp action or topological charge per length of world line measurable in the confinement phase. The *ensemble* averages of these quantities coincide for time-like and space-like currents within the variances. The ensemble variances and averages are considerably larger than the corresponding ones obtained for the remaining cubes which are dual to empty links.

Secondly, let us consider the case of deconfinement (Fig. 11). We have found only one configuration carrying a non-vanishing total topological charge. This is the configuration which stands out by the cross jumped up in the lower left figure. This configuration has only time-like monopoles. One of the static monopoles is exactly located at the center of the topological charge lump which fluctuates but persists over all Euclidean time slices. This

object determines the total charge $Q = 1$. The opposite static antimonopole sits in a topologically non-active part of the lattice. In the high temperature ensemble, there are only four configurations in total which contain space-like monopole currents (the circles in the left plots of the figure). Only for these configurations we can estimate an action per length of space-like monopoles. In spite of the low statistics, this points towards a lower action of space-like monopole currents than that of time-like monopoles at this temperature, in accordance to Fig. 7. Only for time-like monopole currents (mostly belonging to perfectly static monopoles) the averages of local action are markedly bigger than the respective quantities for cubes which are dual to empty links. For the absolute value of the local topological charge the situation is not so clear.

The static monopoles in the deconfinement phase are particle-like excitations possibly amenable to a semi-classical description. On the contrary, discussing Fig. 10 we have seen that in the confinement phase quantities like mean action or mean topological charge per length of monopole world line fluctuate strongly from configuration to configuration. Therefore, a semi-classical treatment of the Abelian monopoles seems to be questionable in the confinement phase.

Finally, in Fig. 12 the total length of monopole loops is shown, separated into the time-like and space-like part, for each individual lattice field configuration at $\beta = 1.4$ and $\beta = 1.8$, respectively. In the confinement phase space-like monopole currents dominate over time-like although there exists, at finite temperature, already some anisotropy (the ratio is smaller than 3). We find large clusters of monopole currents which percolate through the lattice both in time *and* in the three space directions. This will be the topic of a separate publication [25]. In the deconfinement phase only monopole-antimonopole pairs remain where each world line wraps around the time direction. In our sample, space-like currents occur exclusively as deformations of these *almost static* world lines, only in the four configurations mentioned above. This is clearly visible in Fig. 12 and illustrates the direction in which the monopole content of the theory is changed in the deconfinement phase. Nearer to the transition temperature we expect space-like monopole currents to occur more

frequently but no space-like percolation should exist above the transition temperature.

VI. CONCLUSIONS

In this paper we have discussed in detail the topological structure of pure $SU(2)$ lattice gauge theory at finite temperature. We have analyzed lattice configurations simultaneously with respect to instanton-like topological excitations and with respect to Abelian monopoles (within the maximally Abelian gauge). We have employed the framework of recently developed classically perfect actions, more precisely a truncated fixed-point action. Ultraviolet fluctuations were suppressed by techniques which play an important constructive role within the perfect action improvement program itself - blocking and inverse blocking transformations ('smoothing'). In contrast to various action minimization schemes classified as 'cooling', smoothing represents just one controllable constrained minimization step, which keeps the smoothed fields close to the blocked fields at scale $2a$.

We have seen that the result of 'smoothing', nevertheless, looks quite similar to that of 'cooling', if one restricts the latter to very few and/or small iteration steps. The topological structure becomes already clearly visible in terms of clusters of action and topological charge ranging over several lattice spacings. These clusters are certainly poorly described by ideal classical instanton solutions, but inside these clusters action and topological charge vary continuously. At positions of high action density the smoothed gauge fields turn out to be preferentially locally selfdual or anti-selfdual.

We have further investigated the correlation between instanton-like excitations and Abelian monopoles which can be found after maximally Abelian gauge fixing and Abelian projection. In order to illustrate this we have presented different views on the local correlation by examining pieces of monopole world lines with respect to action and topological charge densities attached to them.

We found that despite their detection within the maximally Abelian gauge, monopole currents alter the probability distributions of locally defined gauge independent quantities

like action and topological density. Monopoles carry, in a statistical sense, significantly more gauge-invariant quantities like action and topological charge, which might indicate that the dual superconductor mechanism has a gauge-invariant explanation. This is in the spirit of a recent investigation reported in Ref. [26]. The signal becomes enhanced for smoothed configurations.

Independent of the *density* of monopole currents (being strongly reduced by smoothing) the relevant signal for monopole condensation is percolation in all Euclidean directions. In particular, spatial percolation seems to be needed to produce confinement in the usual sense, *i.e.* the area law of time-like Wilson loops. The monopole content also of smoothed configurations fulfills this criterion in the confinement phase. Concerning deconfinement, we have seen at large β that exclusively almost static monopole-like objects remain after smoothing. They can still explain magnetic screening (the area law of space-like Wilson loops) in this phase.

For the near future we plan to investigate Abelian dominance after smoothing and to analyze the structure of the remaining dilute monopole currents in more detail. We shall try to understand in as far the contribution of Abelian monopoles can quantitatively account for the area law of large Wilson loops. We hope to be able to determine physically relevant scales like the average extension of and the distance between instanton- and/or monopole-like clusters.

Acknowledgments

We are very indebted to the members of the Boulder group, in particular to T. G. Kovacs, who forwarded their new parametrization of the $SU(2)$ fixed-point action to us prior to publication. S. T. would like to thank M. Feurstein for stimulating discussions. E.-M. I., H. M. and M. M.-P. gratefully acknowledge the kind hospitality of T. Suzuki and all other organizers of the *1997 Yukawa International Seminar (YKIS'97)* on *Non-Perturbative QCD - Structure of the QCD Vacuum* - at the Yukawa Institute for Theoretical Physics of Kyoto

University.

---

[1] G. 't Hooft, Phys. Rev. **D 14,** 3432 (1976).

[2] C. G. Callan, R. Dashen, and D. J. Gross, Phys. Rev. **D 17,** 2717 (1978);
D. J. Gross, R. D. Pisarski, and L. G. Yaffe, Rev. Mod. Phys. **53,** 43 (1981).

[3] D. I. Diakonov and V. Yu. Petrov, Nucl. Phys. **B 245,** 259 (1984);
D. I. Diakonov, V. Yu. Petrov, and P. V. Pobylitsa, Phys. Lett. **B 226,** 471 (1989);
D. I. Diakonov, *e-print archive* hep-ph/9602375.

[4] E. Shuryak, Phys. Reports **264,** 357 (1996);
T. Schäfer and E. V. Shuryak, Phys. Rev. **D 54,** 1099 (1996);
T. Schäfer and E. V. Shuryak, Phys. Rev. **D 53,** 6522 (1996);
T. Schäfer and E. V. Shuryak, *e-print archive* hep-ph/9610451.

[5] G. 't Hooft, Nucl. Phys. **B 190,** 455 (1981).

[6] S. Mandelstam, Phys. Reports **23 C,** 245 (1976).

[7] A. S. Kronfeld, G. Schierholz, and U.-J. Wiese, Nucl. Phys. **B 293,** 461 (1987);
A. S. Kronfeld, M. L. Laursen, G. Schierholz, and U.-J. Wiese, Phys. Lett. **B 198,** 516 (1987).

[8] T. Suzuki and I. Yotsuyanagi, Phys. Rev. **D 42,** 4257 (1990).

[9] G. S. Bali, V. Bornyakov, M. Müller-Preussker, and K. Schilling, Phys. Rev. **D 54,** 2863 (1990).

[10] L. Del Debbio, A. Di Giacomo, G. Paffuti, and P. Pieri, Nucl. Phys. **B** (Proc. Suppl.) **42,** 234 (1995);
L. Del Debbio, A. Di Giacomo, G. Paffuti, and P. Pieri, Phys. Lett. **B 355,** 255 (1995).

[11] M. N. Chernodub, M. I. Polikarpov, and A. I. Veselov, Nucl. Phys. **B** (Proc. Suppl.) **47,** 307

(1996);

M. N. Chernodub, M. I. Polikarpov, and A. I. Veselov, *e-print archive* hep-lat/9610007;

A. I. Veselov, M. I. Polikarpov, and M. N. Chernodub, JETP Lett. **63,** 411 (1996).

[12] V. G. Bornyakov and G. Schierholz, Phys. Lett. **B 384,** 190 (1996).

[13] S. Thurner, M. Feurstein, H. Markum, and W. Sakuler, Phys. Rev. **D 54,** 3457 (1996);

S. Thurner, H. Markum, and W. Sakuler, *in Proceedings of* Confinement 95, Osaka 1995, eds. H. Toki *et al.* (World Scientific, 1996) 77;

H. Markum, W. Sakuler, and S. Thurner, Nucl. Phys. **B** (Proc. Suppl.) **47,** 254 (1996).

[14] R. C. Brower, K. N. Orginos, and C.–I Tan, Nucl. Phys. **B** (Proc. Suppl.) **53,** 488 (1997);

R. C. Brower, K. N. Orginos, and C.–I Tan, *e-print archive* hep-th/9610101.

[15] T. DeGrand, A. Hasenfratz, P. Hasenfratz, and F. Niedermayer, Nucl. Phys. **B 454,** 587 (1995).

[16] T. A. DeGrand, A. Hasenfratz, P. Hasenfratz, F. Niedermayer, and U.-J. Wiese, Nucl. Phys. **B** (Proc. Suppl.) **42,** 67 (1995);

T. DeGrand, A. Hasenfratz, P. Hasenfratz, and F. Niedermayer, Nucl. Phys. **B 454,** 615 (1995);

T. DeGrand, A. Hasenfratz, P. Hasenfratz, and F. Niedermayer, Phys. Lett. **B 365,** 233 (1996);

M. Blatter and F. Niedermayer, Nucl. Phys. **B 482,** 286 (1996).

[17] T. A. DeGrand, A. Hasenfratz, and De-cai Zhu, Nucl. Phys. **B 475,** 321 (1996);

T. A. DeGrand, A. Hasenfratz, and De-cai Zhu, Nucl. Phys. **B 478,** 349 (1996).

[18] P. Hasenfratz and F. Niedermayer, Nucl. Phys. **B 414,** 785 (1994).

[19] M. Feurstein, E.-M. Ilgenfritz, M. Müller-Preussker, and S. Thurner, Nucl. Phys. **B 511,** 421 (1998).

[20] T. DeGrand, A. Hasenfratz, and T. G. Kovacs, Nucl. Phys. **B 505,** 417 (1997).

[21] T. G. Kovacs, *private communication.*

[22] J. Engels, J. Fingberg, and M. Weber Nucl. Phys. **B 332,** 737 (1990).

[23] M. Lüscher, Comm. Math. Phys. **85,** 39 (1982).

[24] T. A. DeGrand and D. Toussaint, Phys. Rev. **D 22,** 2478 (1980).

[25] E.-M. Ilgenfritz, H. Markum, M. Müller-Preussker, and S. Thurner, *in preparation.*

[26] B. L. G. Bakker, M. N. Chernodub, and M. I. Polikarpov, Phys. Rev. Lett. **80,** 30 (1998).

TABLES:

$w(i,j)$	$j=1$	$j=2$	$j=3$	$j=4$
$i=1$ (plaquettes)	1.115504	$-.5424815$	.1845878	$-.01197482$
$i=2$ (6-link loops)	$-.01443798$	.1386238	$-.07551325$	.01579434

TABLE I. Weight coefficients of the simplified fixed-point action

FIGURE CAPTIONS:

FIG. 1: Monte Carlo histories of the blocked action $S_{FP}(V)$ and of the extended action $S_{FP}(U^{SM}) + \kappa T(U^{SM}, V)$ for the smoothed configurations on a 12^4 lattice at $\beta = 2.5$ as a test for the action to be used in this work.

FIG. 2: Binder cumulants for the Polyakov loops before and after blocking.

FIG. 3: Monte Carlo sequence from the confinement phase at $\beta = 1.4$ of topological charges in the smoothed configurations according to the naive and Lüscher's charge.

FIG. 4: (a) Clustering of topological density $q(x)$ after smoothing for a confinement configuration with $Q = 0$ obtained at $\beta = 1.4$. The subplots show xy-slices for $t = 1, \cdots, 4$ and $z = 1, \cdots, 6$. Monopole currents are drawn as arrows. Time-like (anti-) monopoles are symbolized by arrows to (from) the upper right, space-like (anti-) monopoles with world lines in the z direction by arrows to (from) the upper left. (b) Same as (a) for $z = 7, \cdots, 12$. (c) Clustering of topological density $q(x)$ after smoothing for a deconfinement configuration with $Q = 0$ obtained at $\beta = 1.8$. The subplots show xy-slices for $t = 1, \cdots, 4$ and $z = 1, \cdots, 6$. (d) Same as (c) for $z = 7, \cdots, 12$.

FIG. 5: Probability distributions for finding a local topological charge $q(x)$ at a lattice site together with a given local action $s_{site}(x)$. 50 independent confinement configurations obtained at $\beta = 1.4$ have been analyzed and the q distributions are separately normalized for all values of s_{site}.

FIG. 6: Average occupation number of magnetic monopoles $\langle m \rangle$ on nearest dual links, de-

pending on the local action $s_{site}(x)$ (upper plot) and depending on the topological density $q(x)$ (lower plot). The figure depicts the situation in the confinement phase at $\beta = 1.4$, being similar to the deconfinement phase.

FIG. 7: Probability distributions for the action $s_{3-cube}(c)$ living on a 3-cube depending on whether the dual link is occupied ($m = 1$) by a monopole current or not ($m = 0$). A distinction between time-like and space-like monopoles is made. 50 independent configurations have been analyzed in both phases at $\beta = 1.4$ and $\beta = 1.8$. The average values $\langle s_{3-cube}(c)\rangle$ and the square roots of the variances $\sqrt{\langle \Delta s_{3-cube}(c)^2\rangle}$ are inserted.

FIG. 8: Probability distributions for a local topological charge (summed over the 8 corners of a 3-cube) depending on whether the dual link is occupied ($m = 1$) by a monopole current or not ($m = 0$). The representation is the same as in the previous figure.

FIG. 9: Same as previous two figures but for unsmoothed configurations at $\beta = 1.4$ in the confinement phase.

FIG. 10: Mean local action s_{3-cube} and Luescher's hypercube charge for the sequence of Monte Carlo configurations depending on the monopole currents $|m| = 1$ or 0 on space-like and time-like dual links in the confinement phase at $\beta = 1.4$.

FIG. 11: Same as previous figure in the deconfinement phase at $\beta = 1.8$. Note the isolated point in the lower left plot is due to $Q = 1$.

FIG. 12: Monopole lengths for the sequence of Monte Carlo configurations in the same samples of 50 independent gauge field configurations for both phases ($\beta = 1.4$ and $\beta = 1.8$) as in the previous two figures. Distinction between time-like and space-like currents is made.

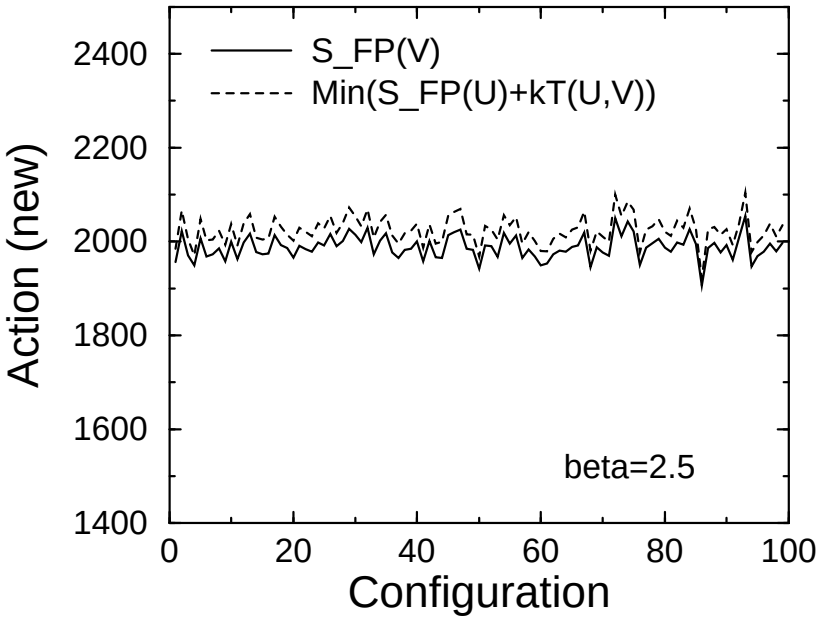
S_FP(V)
Min(S_FP(U)+kT(U,V))
beta=2.5
Action (new)
Configuration
2400
2200
2000
1800
1600
1400
0
20
40
60
80
100

FIG. 1

before blocking

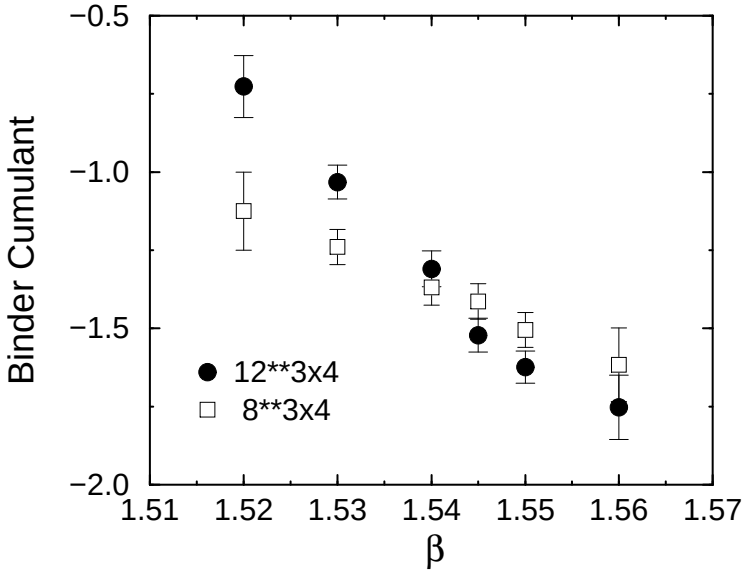

after blocking

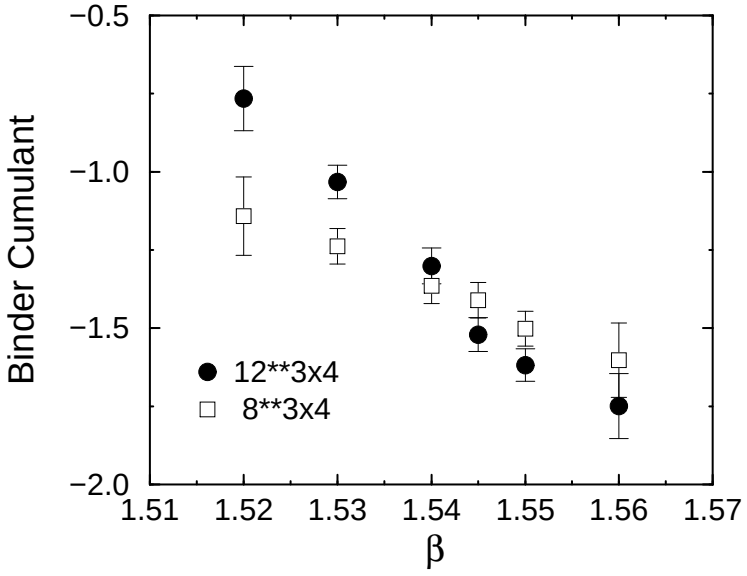

FIG. 2

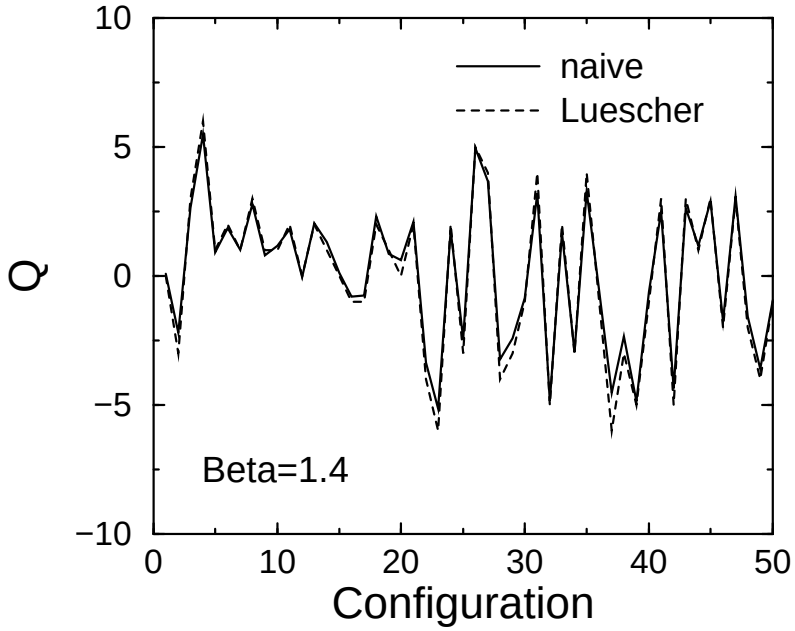
10
5
0
−5
−10
Q
0
10
20
30
40
50
Configuration
naive
Luescher
Beta=1.4

FIG. 3

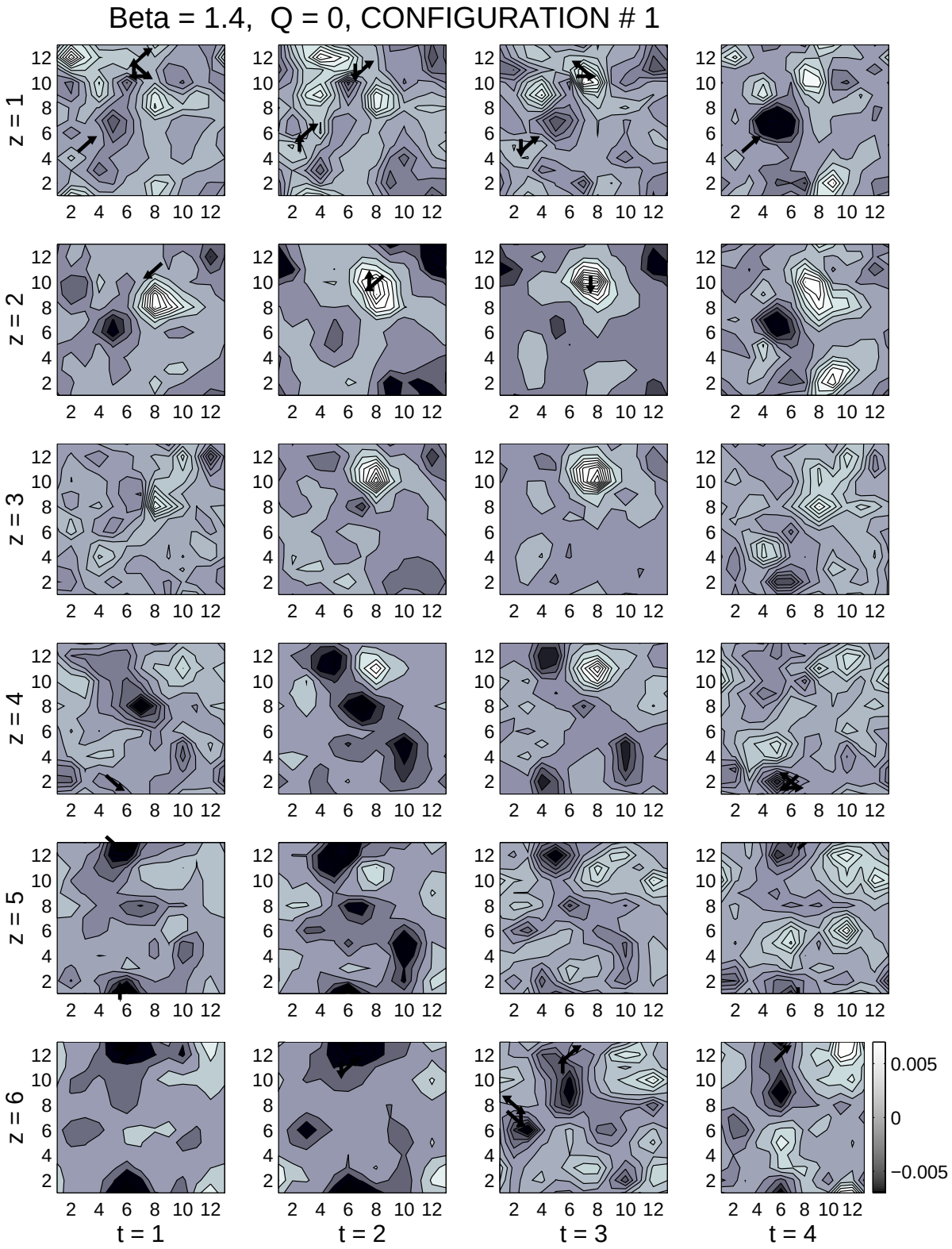
Beta = 1.4, Q = 0, CONFIGURATION # 1
z = 1
z = 2
z = 3
z = 4
z = 5
z = 6
t = 1
t = 2
t = 3
t = 4
0.005
0
−0.005

FIG. 4a

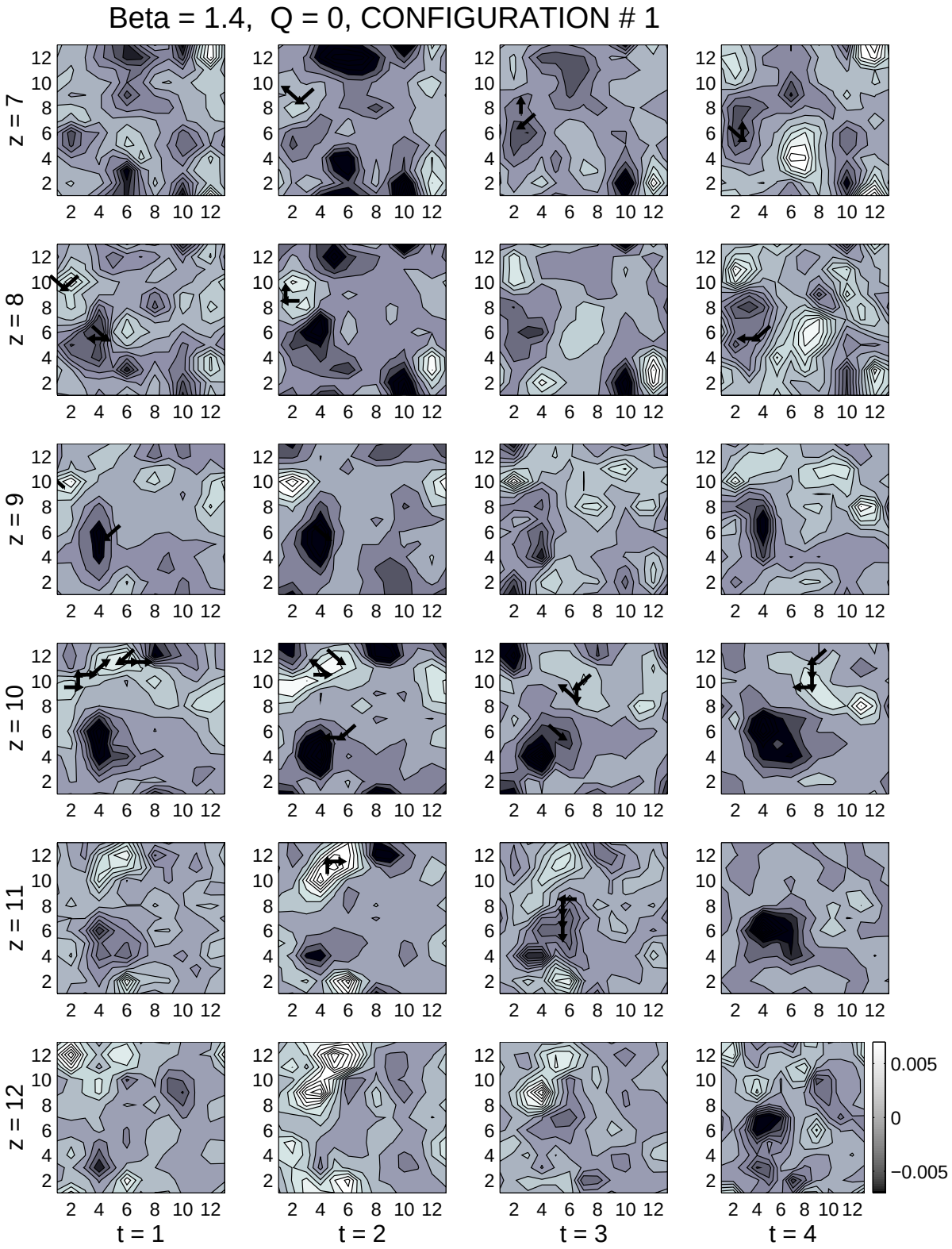
Beta = 1.4, Q = 0, CONFIGURATION # 1
z = 7
z = 8
z = 9
z = 10
z = 11
z = 12
t = 1
t = 2
t = 3
t = 4
0.005
0
−0.005

FIG. 4b

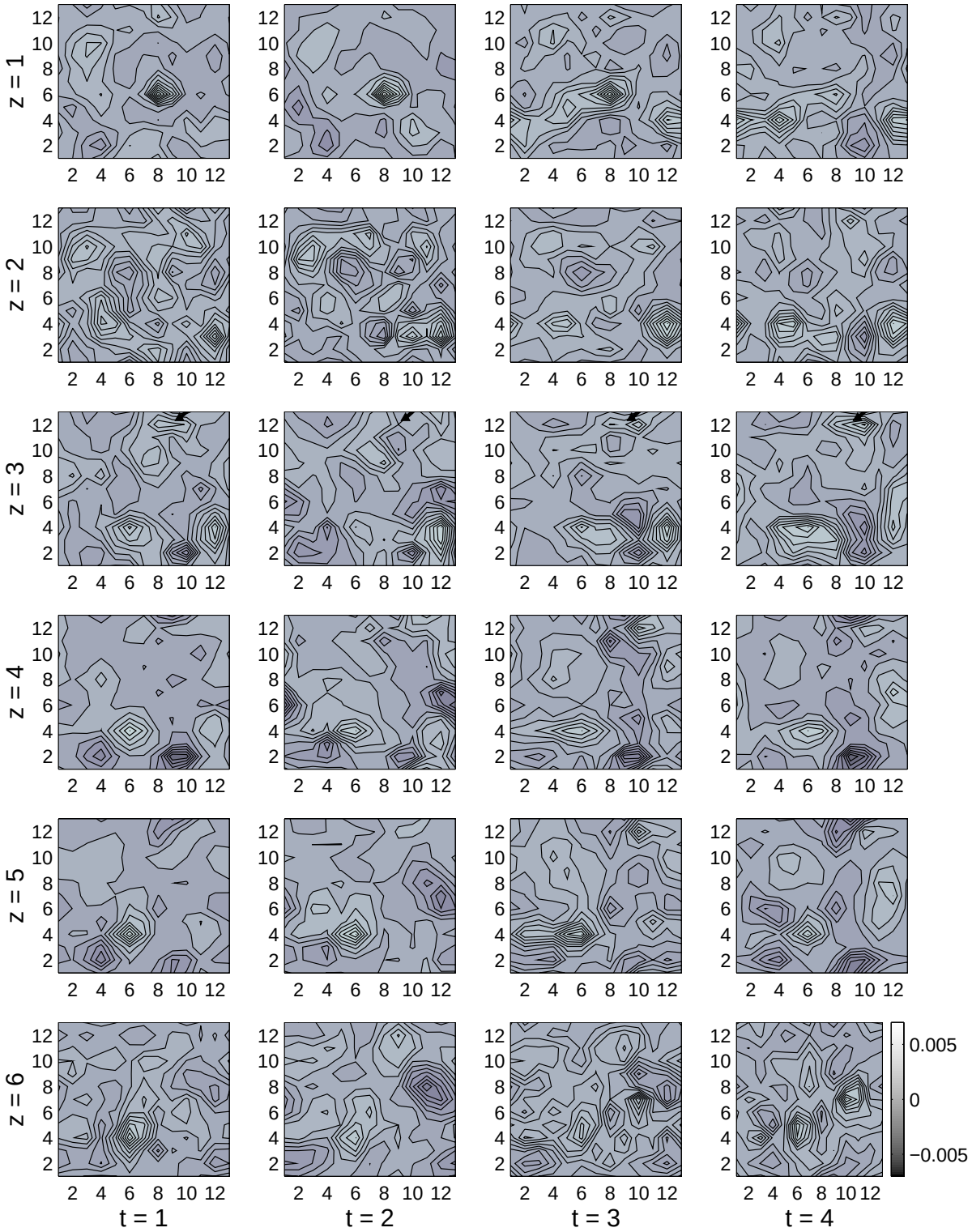
Beta = 1.8, Q = 0, CONFIGURATION # 5
z = 1
z = 2
z = 3
z = 4
z = 5
z = 6
t = 1
t = 2
t = 3
t = 4
0.005
0
−0.005

FIG. 4c

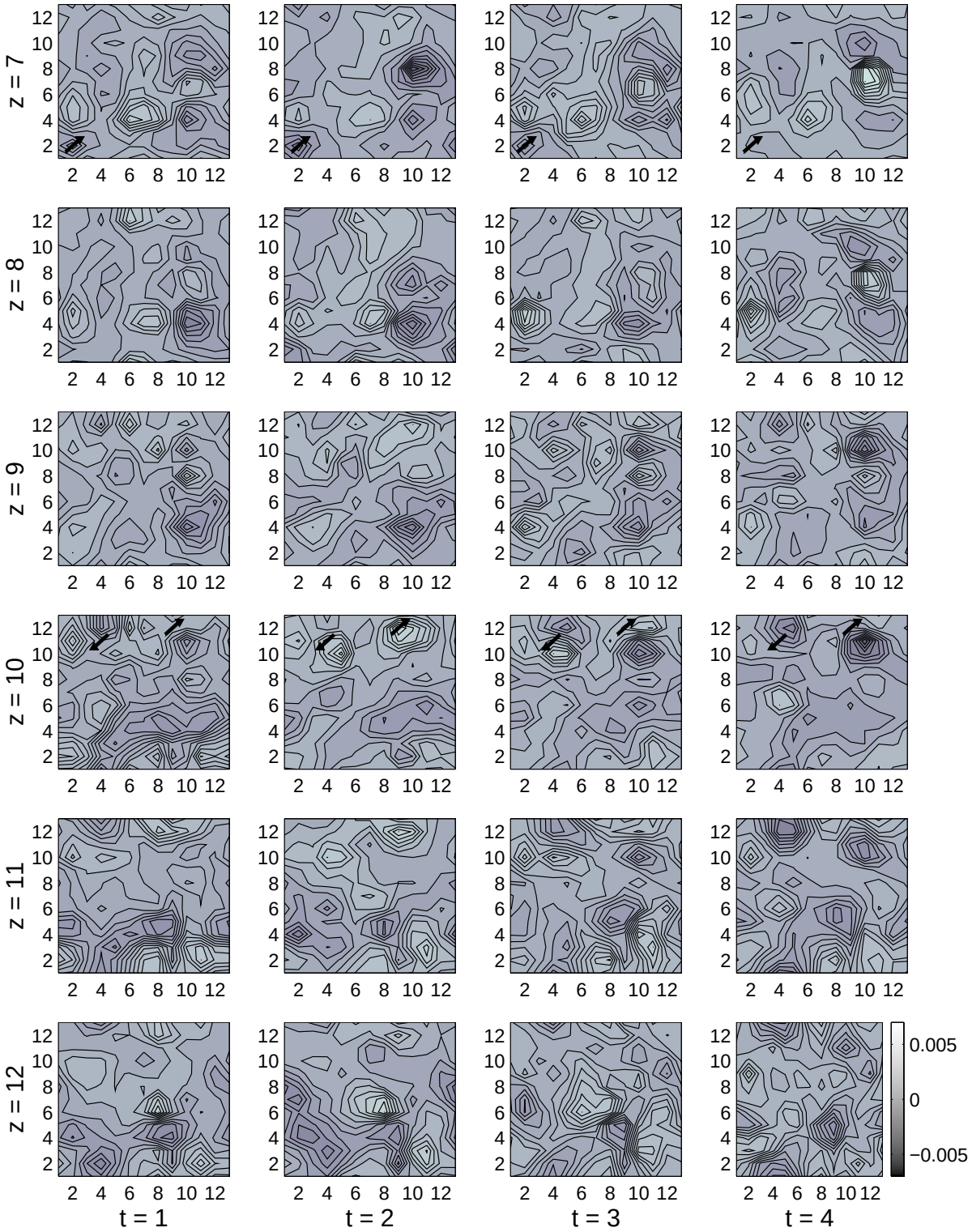
Beta = 1.8, Q = 0, CONFIGURATION # 5
z = 7
z = 8
z = 9
z = 10
z = 11
z = 12
t = 1
t = 2
t = 3
t = 4
0.005
0
−0.005

FIG. 4d

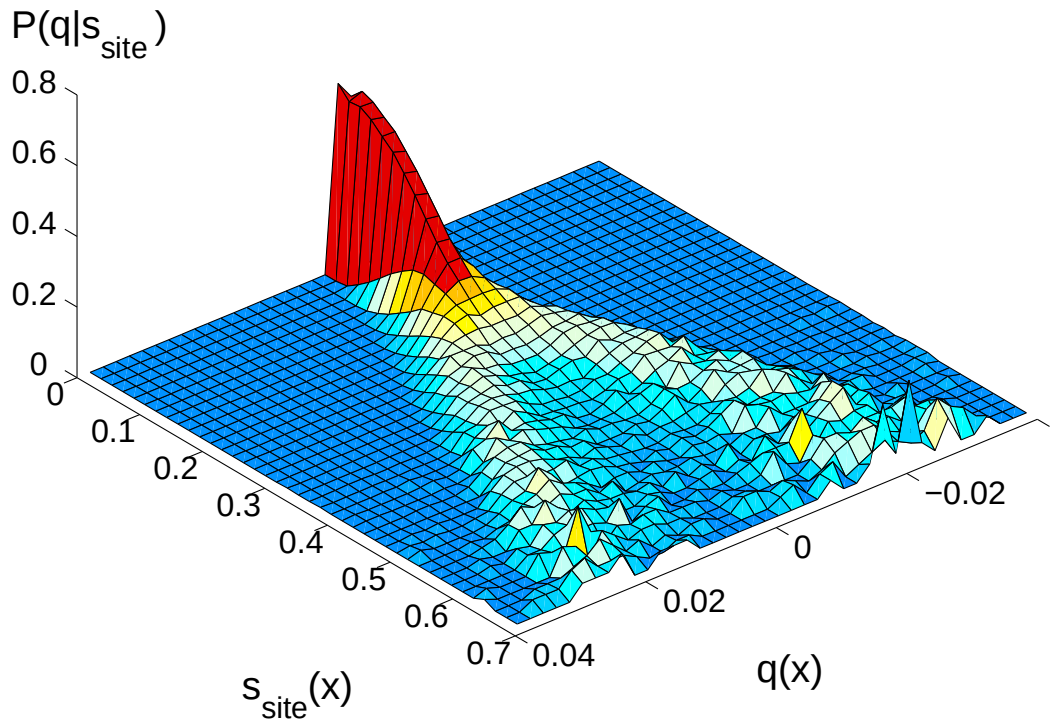
BETA=1.40
P(q|s site)
0.8
0.6
0.4
0.2
0
0
0.1
0.2
0.3
0.4
0.5
0.6
0.7
s site (x)
0.04
0.02
0
−0.02
q(x)

FIG. 5

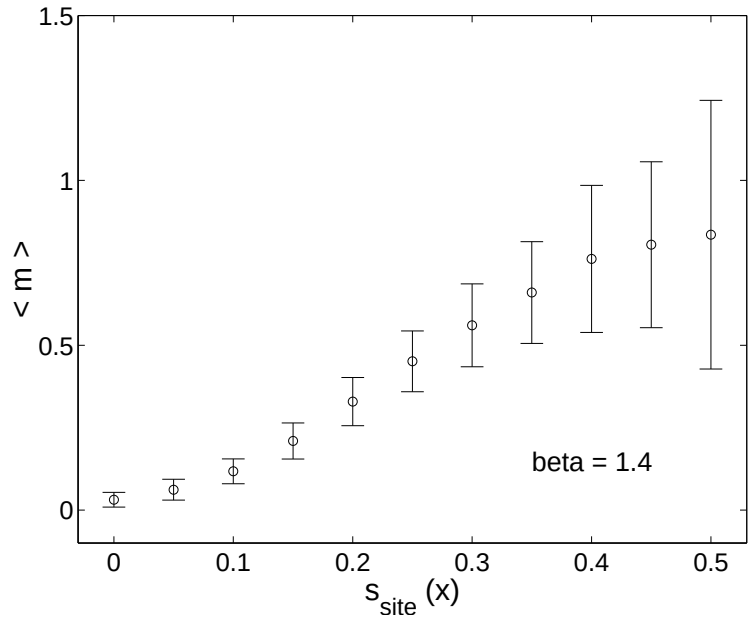
1.5
1
0.5
0
< m >
beta = 1.4
0
0.1
0.2
0.3
0.4
0.5
s_site (x)

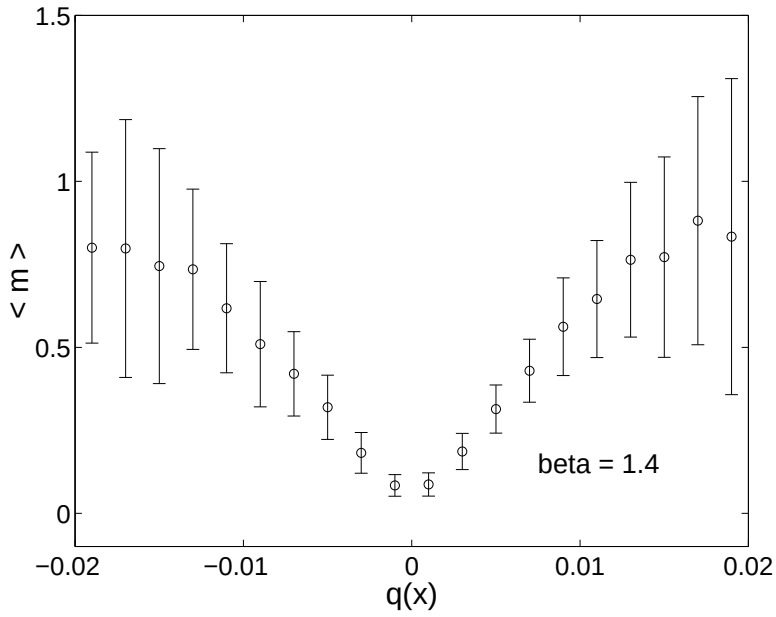
1.5
1
0.5
0
< m >
beta = 1.4
−0.02
−0.01
0
0.01
0.02
q(x)

FIG. 6

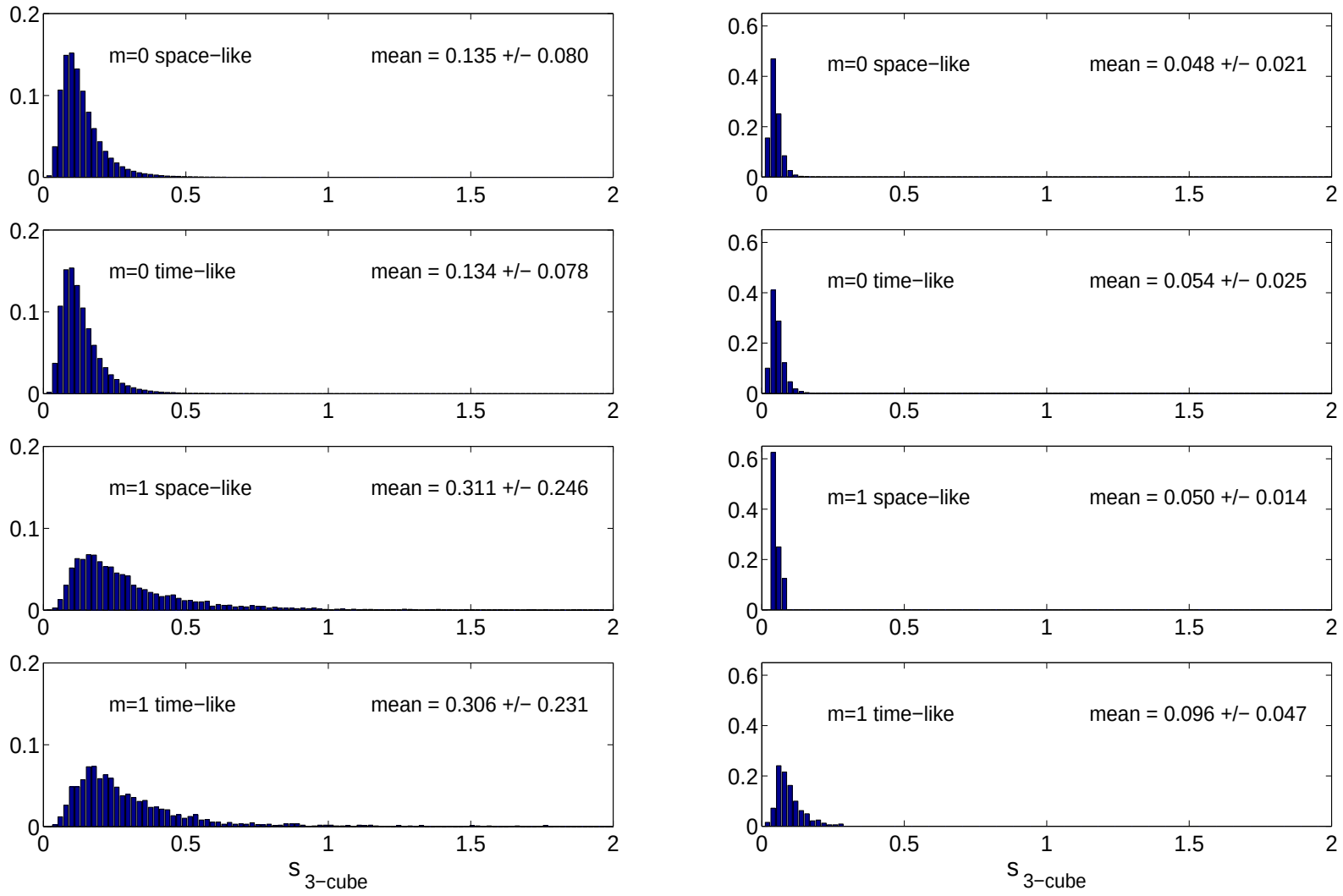
Action, beta=1.4
Action, beta=1.8
m=0 space−like
mean = 0.135 +/− 0.080
m=0 time−like
mean = 0.134 +/− 0.078
m=1 space−like
mean = 0.311 +/− 0.246
m=1 time−like
mean = 0.306 +/− 0.231
m=0 space−like
mean = 0.048 +/− 0.021
m=0 time−like
mean = 0.054 +/− 0.025
m=1 space−like
mean = 0.050 +/− 0.014
m=1 time−like
mean = 0.096 +/− 0.047
s 3−cube
s 3−cube

FIG. 7

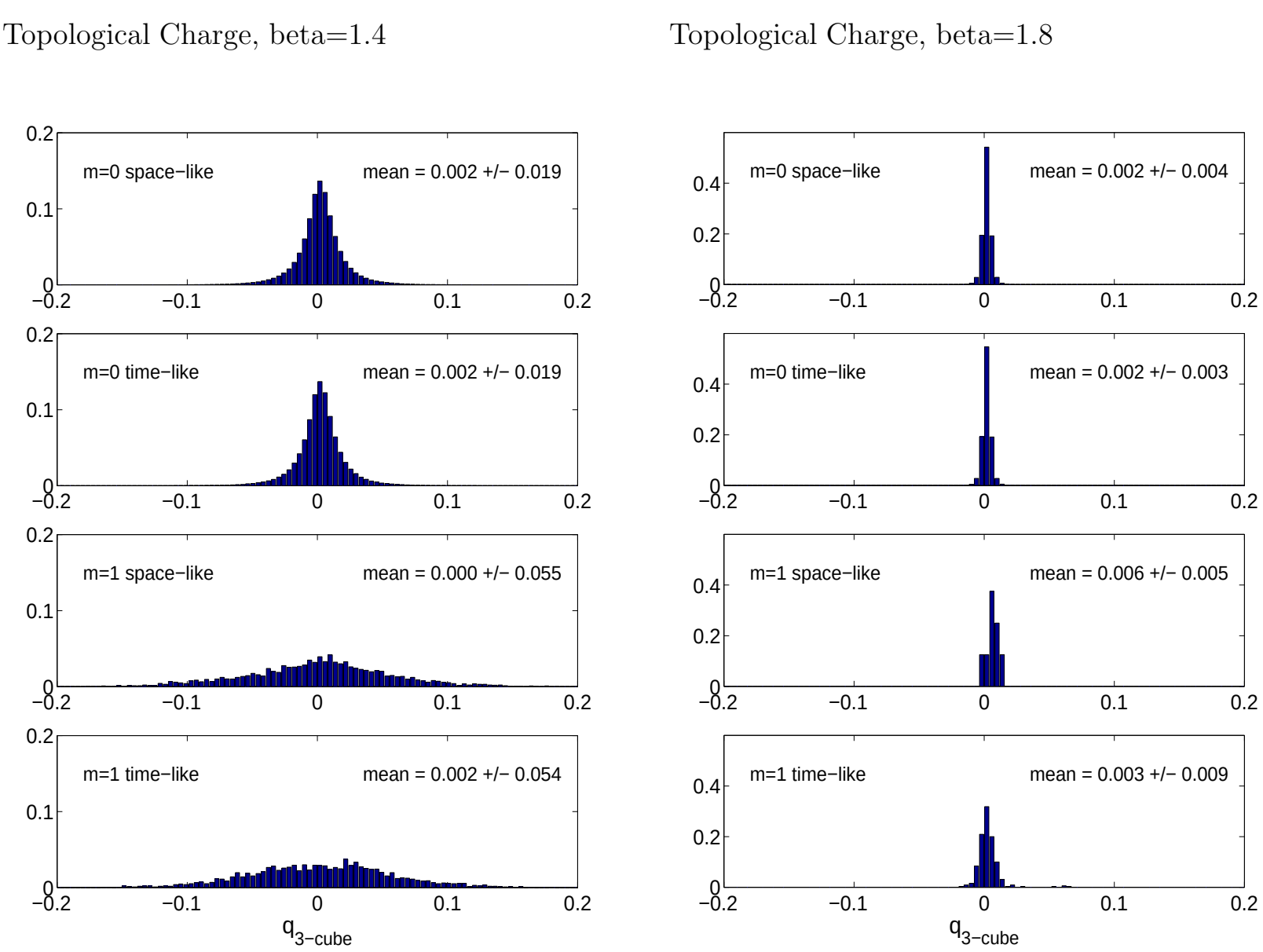
Topological Charge, beta=1.4
Topological Charge, beta=1.8
m=0 space−like
mean = 0.002 +/− 0.019
m=0 time−like
mean = 0.002 +/− 0.019
m=1 space−like
mean = 0.000 +/− 0.055
m=1 time−like
mean = 0.002 +/− 0.054
m=0 space−like
mean = 0.002 +/− 0.004
m=0 time−like
mean = 0.002 +/− 0.003
m=1 space−like
mean = 0.006 +/− 0.005
m=1 time−like
mean = 0.003 +/− 0.009
q3−cube
q3−cube

FIG. 8

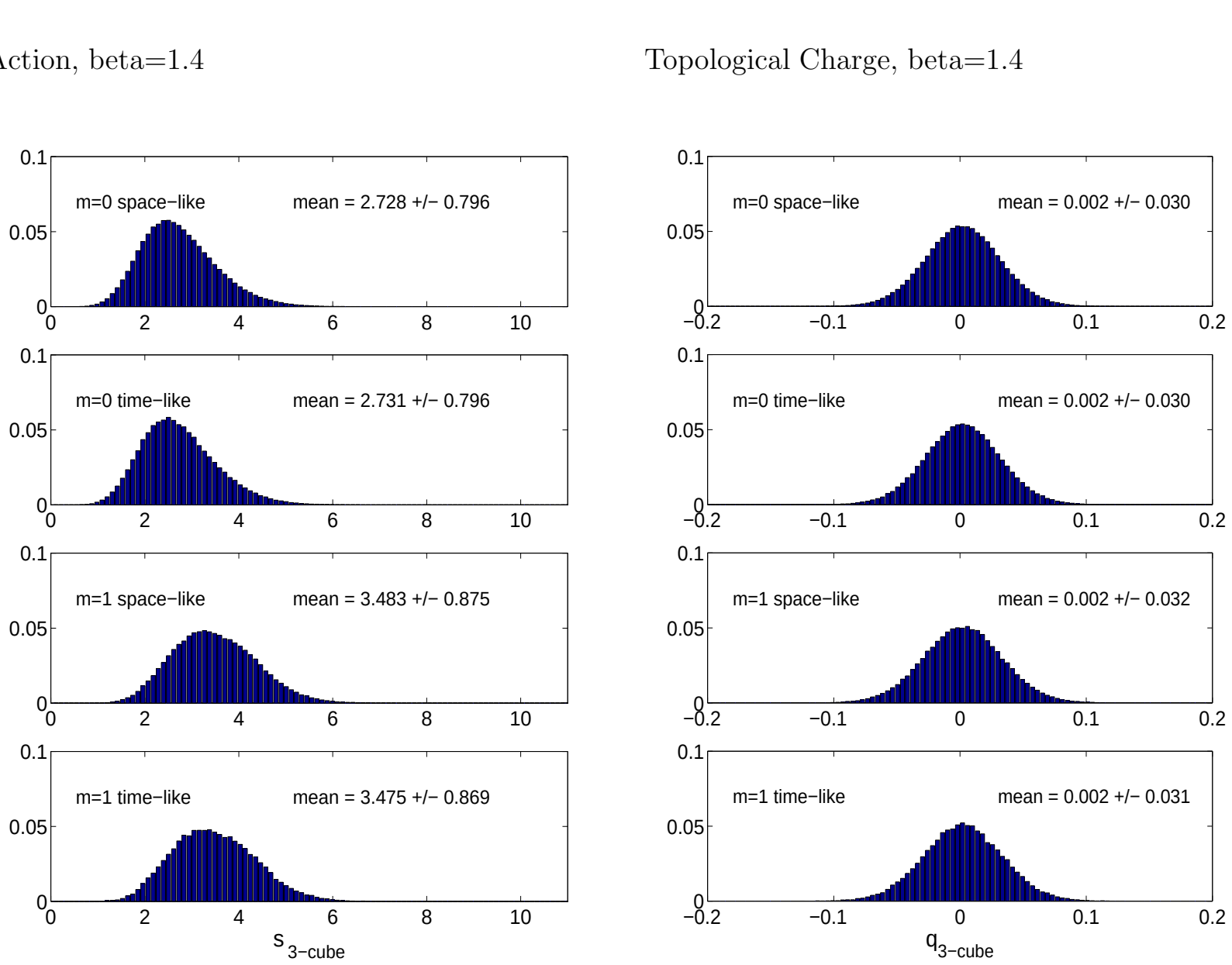
Action, beta=1.4
Topological Charge, beta=1.4
m=0 space−like
mean = 2.728 +/− 0.796
m=0 time−like
mean = 2.731 +/− 0.796
m=1 space−like
mean = 3.483 +/− 0.875
m=1 time−like
mean = 3.475 +/− 0.869
m=0 space−like
mean = 0.002 +/− 0.030
m=0 time−like
mean = 0.002 +/− 0.030
m=1 space−like
mean = 0.002 +/− 0.032
m=1 time−like
mean = 0.002 +/− 0.031
s 3−cube
q 3−cube

FIG. 9

beta=1.4

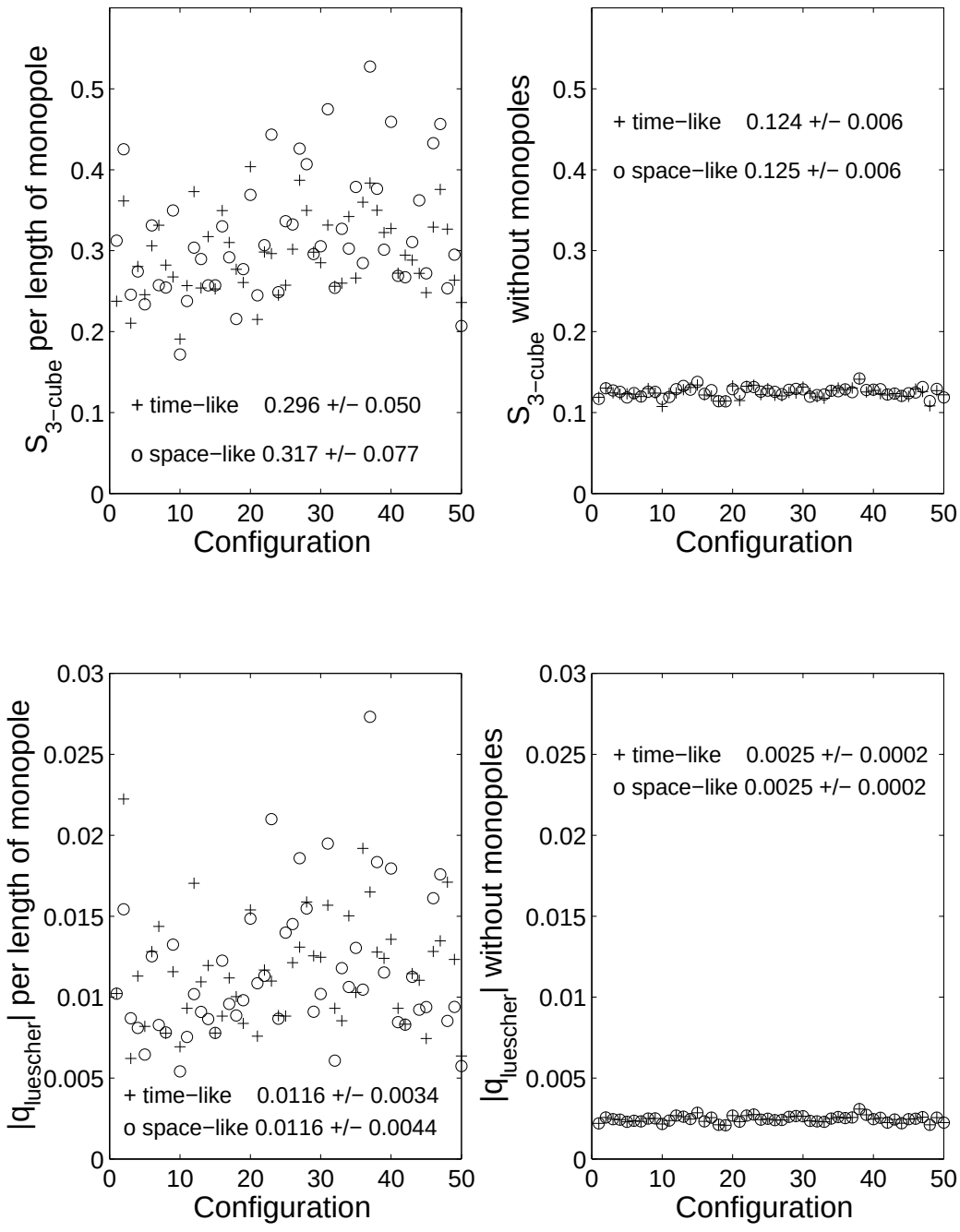

FIG. 10

beta=1.8

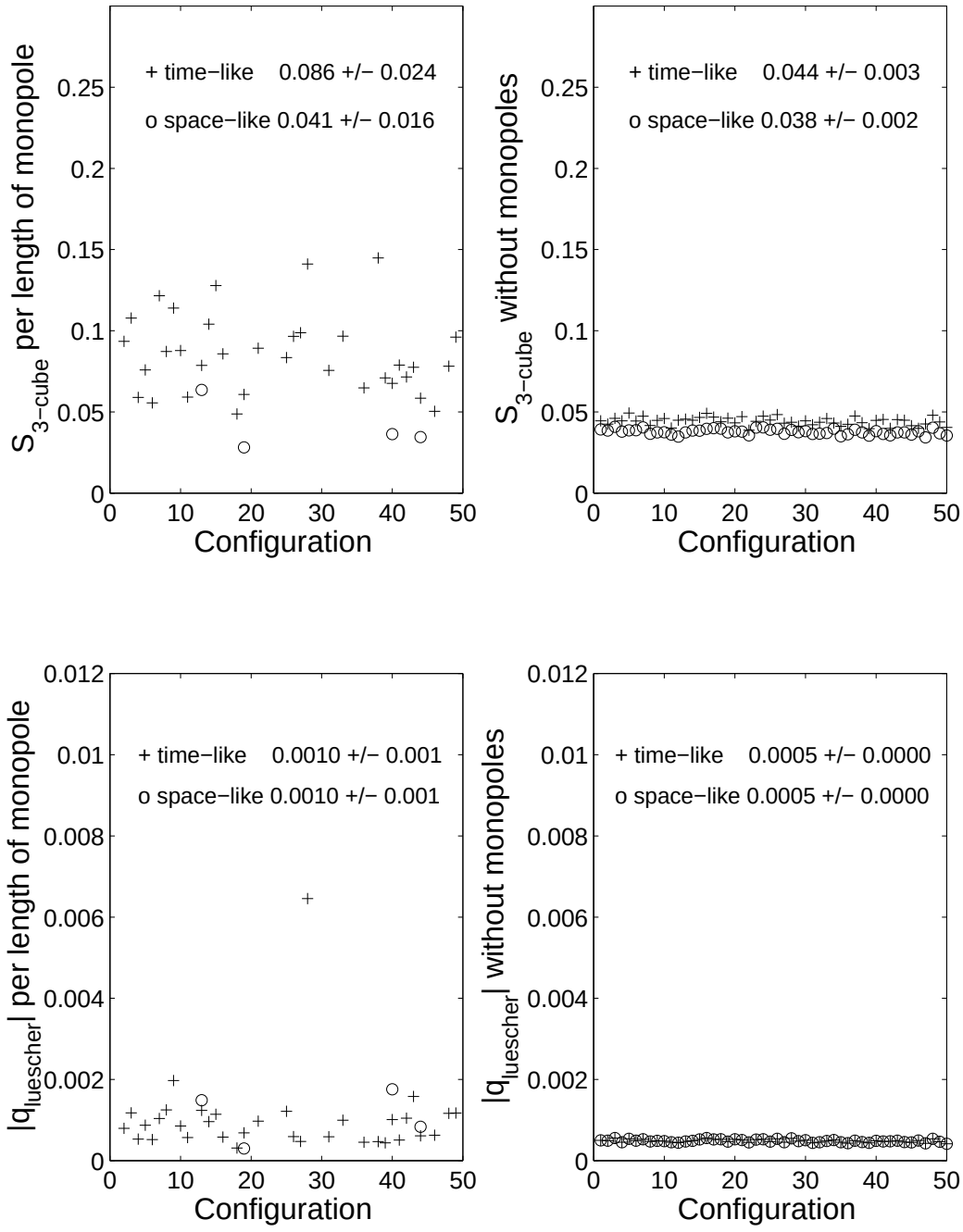

FIG. 11

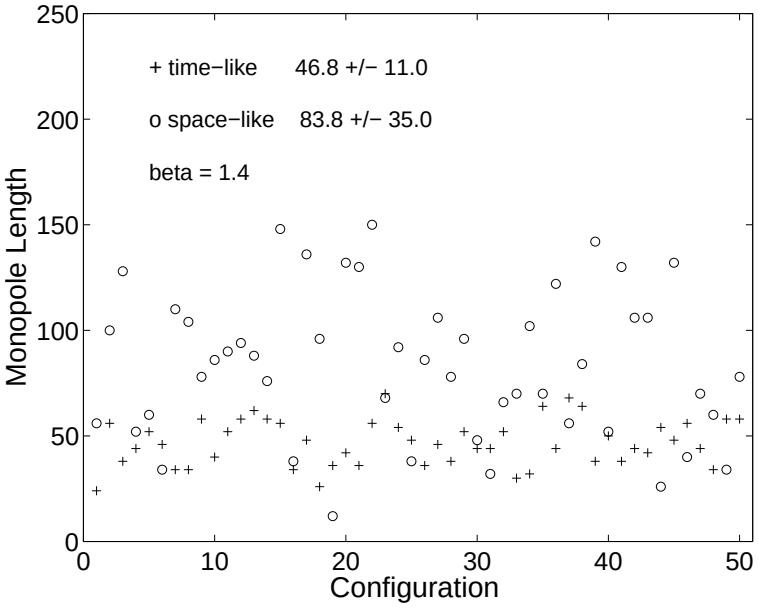
+ time−like 46.8 +/− 11.0
o space−like 83.8 +/− 35.0
beta = 1.4
Monopole Length
Configuration
0
50
100
150
200
250
0
10
20
30
40
50

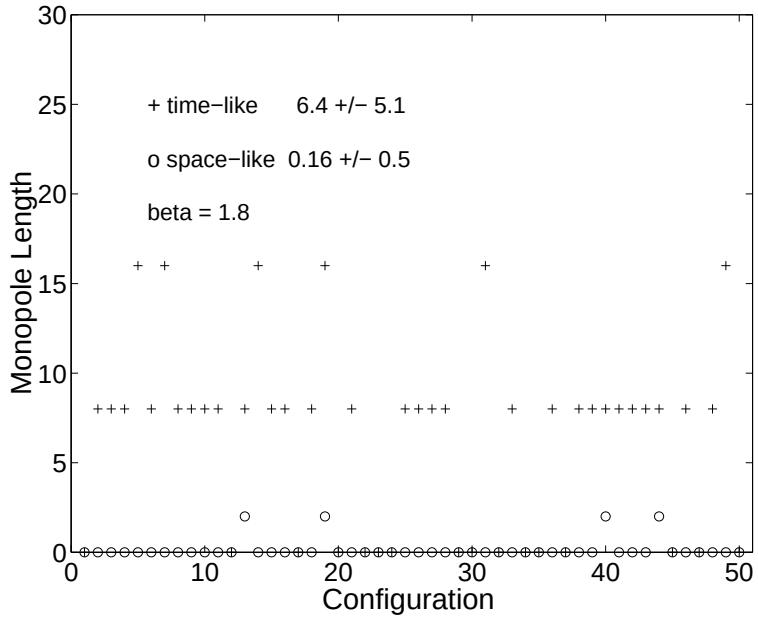
+ time−like 6.4 +/− 5.1
o space−like 0.16 +/− 0.5
beta = 1.8
Monopole Length
Configuration
0
5
10
15
20
25
30
0
10
20
30
40
50

FIG. 12

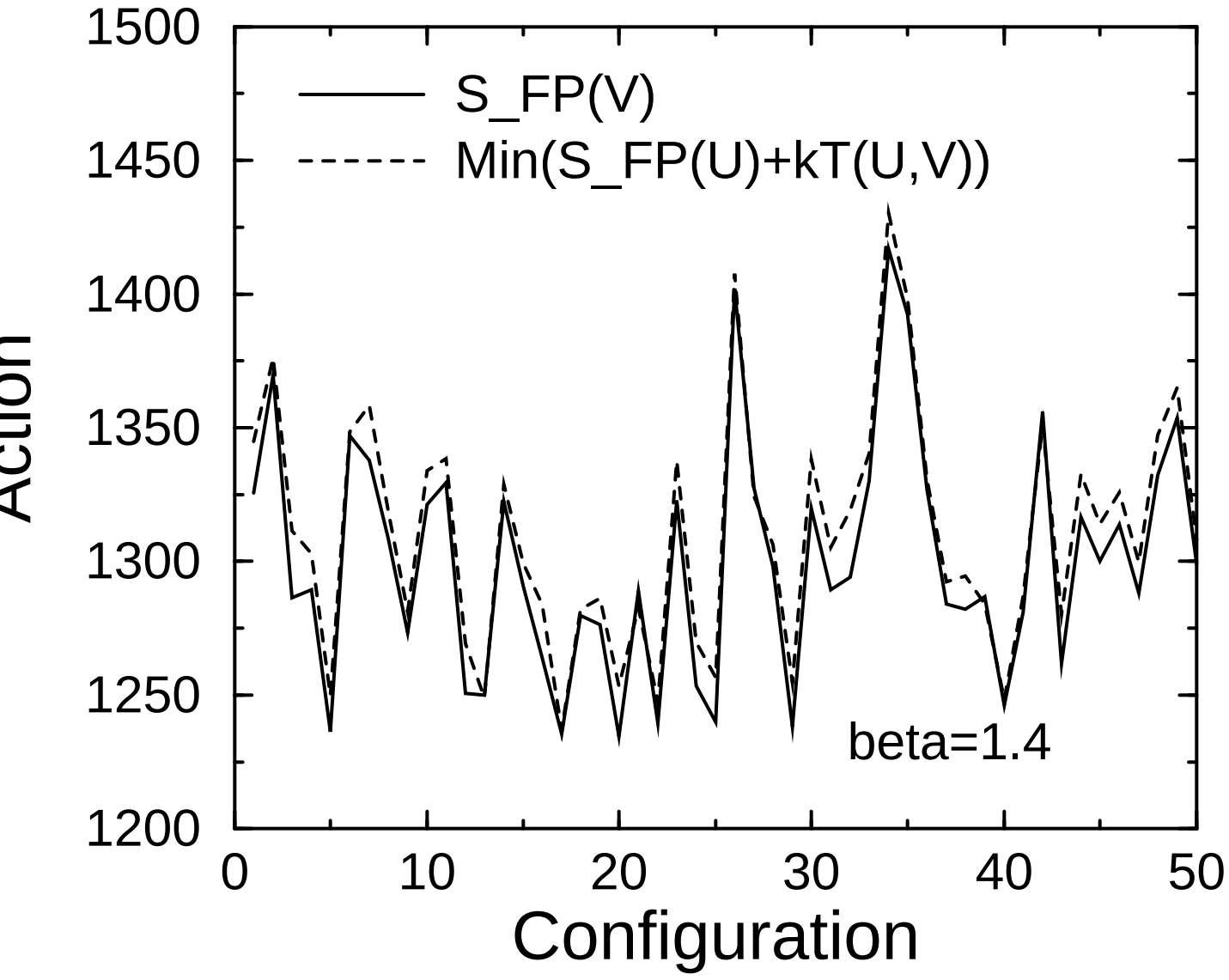
1500
1450
1400
1350
1300
1250
1200
Action
0
10
20
30
40
50
Configuration
S_FP(V)
Min(S_FP(U)+kT(U,V))
beta=1.4